Electronic and magnetic properties of bimetallic $L1_0$ cuboctahedral clusters by means of fully relativistic density-functional-based calculations

R. Cuadrado and R. W. Chantrell

Department of Physics, University of York, York YO10 5DD, United Kingdom

(Received 25 July 2012; revised manuscript received 6 November 2012; published 18 December 2012)

By means of density functional theory and the generalized gradient approximation, we present a structural, electronic, and magnetic study of FePt-, CoPt-, FeAu-, and FePd-based $L1_0$ ordered cuboctahedral nanoparticles, with total numbers of atoms $N_{\text{tot}} = 13, 55, 147$. After a conjugate gradient relaxation, the nanoparticles retain their $L1_0$ symmetry, but the small displacements of the atomic positions tune the electronic and magnetic properties. The value of the total magnetic moment stabilizes as the size increases. We also show that the magnetic anisotropy energy (MAE) depends on the size as well as the position of the Fe-atomic planes in the clusters. We address the influence on the MAE of the surface shape, finding a small in-plane MAE for $(Fe,Co)_{24}Pt_{31}$ nanoparticles.

DOI: 10.1103/PhysRevB.86.224415 PACS number(s): 75.30.Gw, 31.15.A−, 75.75.Lf, 71.15.Mb

I. INTRODUCTION

Current uses of nanometer designed magnetic devices range from biomedical applications,[1–3] catalysis,[4] energy harvesting,[5] to data storage.[6–9] Because of these diverse applications in nanotechnology,[10,11] the development of nanostructured magnetic materials has become a highly active field. Focusing in the field of magnetic recording, a huge amount of experimental and theoretical work has been carried out during the last decade to seek novel approaches to construct advanced materials for ultrahigh-density magnetic storage, with the aim of increasing the state-of-the-art beyond 1 Tbit/in^2.[8,12–15] Most approaches are focused on thin films or multilayers[16–18] and recently on slabs.[19] However, during the last decade has emerged the possibility to use clusters deposited on surfaces[20–26] to increase the recording density. These clusters or nanoparticles (NPs) have properties different from those of bulk alloys due to their reduced surface atomic coordination. In particular, binary $3d$-$5d$ NPs formed by transition metals (TM) such as Fe or Co together with $5d$ noble metals such as Au or Pt allow the possibility to tune the magnetic properties based on an in-depth knowledge of their geometrical[27–29] and magnetic behavior.[23,30,31]

One vital physical quantity in magnetic recording is the magnetic anisotropy energy (MAE) of the storage medium. The MAE determines the tendency of the magnetization to align along some specific axis in solids and clusters. As we have pointed out, binary magnetic NPs based on (Fe,Co)Pt are good candidates for novel magnetic recording media, especially those phases chemically $L1_0$ ordered, where the value of the MAE is of order of 7×10^7erg/cm^3.[32] The trend to higher recording densities requires continuous reduction in the grain size while retaining large values of the factor KV/kT to avoid loss of recorded information due to the onset of superparamagnetic behavior.[33,34] Following the Néel relaxation law,[35] the only way to reduce the size of the NPs avoiding this trouble is through higher values of the MAE. To control this magnetic energy, mainly determined by the spin-orbit coupling (SOC),[36] it is necessary to investigate the structure and the electronic and the magnetic behaviors of these systems. For this purpose, Gambardella *et al.* showed experimental and theoretically that when Co adatoms were deposited onto a Pt(111) surface, they had a MAE of 9 meV/atom arising from the strong SOC induced by the Pt substrate and for unquenched orbital moments.[20] In addition, they increased the number of Co atoms on the metal surface forming NPs that ranged from 3 up to 40 atoms. The results showed that smaller NPs exhibited a higher MAE. These results opened a route to understand and fabricate high-density magnetic recording materials using deposited NPs on surfaces. There are several experimental[37,38] and theoretical[23,28–31,39–44] studies regarding isolated NPs aiming to obtain the best morphologies and magnetic behavior covering monometallic NPs,[23,29,30] binary alloys,[28,41,42,44] and even capped NPs.[31,43] Gruner *et al.* have carried out a total energy study of a wide range of structures of various shapes and sizes for (Fe,Co)Pt NPs (Ref. 28) as well as for Fe(Pd,Ni).[44] It was found that the most energetically favored structures obtained were those of ordered multiply twinned icosahedra and decahedra shapes. Gruner *et al.* have also obtained locally the magnetic moment (MM) for $Fe_{256}B_{296}$, with B = Ni, Pd, Pt, Ir, Au, and as we will see in this work, the tendency to augment the Fe MM in the vicinity of the cluster surface obtained by Gruner is in good agreement with our results.

To obtain the MAE using the framework of density functional theory (DFT) implies a huge computational resource since a fully relativistic (FR) and a full potential (FP) treatment becomes necessary. A widely used approximation to overcome the all-electron (full potential) problem and to do quick and accurate calculations is to substitute the core electrons by a pseudopotential (PP).[45,46] Most of the codes that use the PP approximation use the scalar-relativistic (SR) corrections (Darwin term and mass velocity), but they are not sufficient to address the behavior of magnetic systems because the MAE is mostly controlled by the SOC. Also, the magnetization density vector can vary from point to point in space presenting a spin noncollinearity[47–52]. To overcome this barrier, we have used a fully relativistic pseudopotential (FR-PP) approach implemented recently in the SIESTA code.[53,54]

The (Fe,Co)Pt $L1_0$ based alloys have large uniaxial anisotropy because of the layered structure (see Fig. 1). The purpose of this paper is to investigate the structural, electronic, and magnetic properties of (Fe,Co)Pt and Fe(Au,Pd) $L1_0$ cuboctahedral nanostructured NPs having the total number of atoms N_{tot} = 13, 55, and 147, and to calculate the MAE

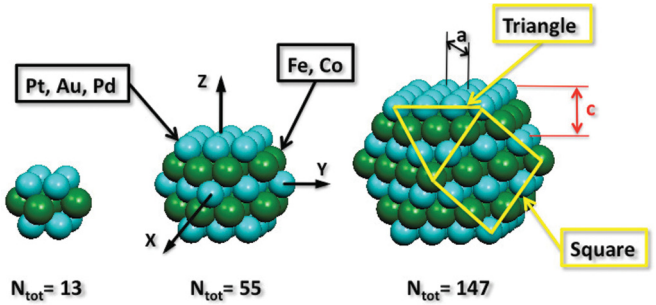

FIG. 1. (Color online) Initial $L1_0$ cuboctahedral structures employed in the simulations. Green spheres depict the magnetic atoms, while turquoise ones are the nonmagnetic species. On the NP at the extreme right, the yellow lines show two kinds of surfaces (square and triangle). The three axes in the second NP ($N_{\rm tot} = 55$) represent the usual Cartesian frame, X,Y,Z being the angles θ and ϕ for each one of them (0°,0°), (90°, 0°) and (90°, 90°), respectively. The distance between planes is marked in red by c parameter and the lattice constant by a.

using the above-mentioned FR-PP scheme. It is shown that the energy surface can become complex, showing features beyond the simple uniaxial anisotropy. This demonstrates the importance of investigating the dependence of the total energy on the orientation of the magnetization axis as we will see in Sec. III D.

The paper is structured as follows. In Sec. II, we describe briefly the theoretical tools to perform all the calculations as well as the kind of NPs studied in this work. The importance of the structural relaxations will be explained in Sec. III A. The local magnetic moments and the density of states are described in Secs. III B and III C, respectively. The MAE and its separate contributions are discussed in Sec. III D. Finally, Sec. IV summarizes the main results.

II. COMPUTATIONAL DETAILS

We have undertaken calculations of electronic structure and magnetic anisotropy energies by means of DFT using a recent fully relativistic implementation[53] in the GREEN (Refs. 55 and 56) code employing the SIESTA (Ref. 54) framework. We use fully separable Kleinmann-Bylander[57] and norm-conserving pseudopotentials of the Troulliers-Martins[58] type to describe the core electrons. Our DFT-based calculations have been performed within the generalized gradient approximation (GGA) for the exchange correlation (XC) potential following the Perdew, Burke, and Ernzerhof (PBE) version.[59] To address the description of magnetic systems, pseudocore (pc) corrections were used to include in the XC terms not only the valence charge density, but also the core charge as Louie *et al.*[61] pointed out. In order to ease the convergence of three center integrals with the size of the real-space grid, $\rho^c(r)$ is replaced by a pseudocore charge density $\rho^{\rm pc}(r)$, which equals the real core charge density beyond a given radius $r_{\rm pc}$, while close to the nuclei it becomes a smooth function. The radius $r_{\rm pc}$ should be chosen small enough to ensure that the overlap region between the valence and the core charges is fully taken into account. Based on previous studies of the binary alloys,[53] we have chosen for the radius that equals the core and valence charge the values of $r_{\rm pc}$(Fe,Co) = 0.6 bohr and $r_{\rm pc}$(Pt,Au,Pd) = 1.0 bohr, ensuring that the overlap region between the valence and the core charge is fully taken into account. As basis set, we have employed double-zeta polarized (DZP) strictly localized numerical atomic orbitals (AO). The confinement energy E_c, defined as the energy cost to confine the wave function within a given radius, was set to 100 meV. The Fermi-Dirac distribution was used to obtain the occupation numbers and the electronic temperature was set to 50 meV.

In the SR pseudopotential approximation, the Kohn-Sham Hamiltonian

$$\hat{H}^{\rm KS} = \hat{T} + \hat{V}^{\rm local} + \hat{V}^{\rm KB} + \hat{V}_H + \hat{V}_{\rm XC} \qquad (1)$$

is diagonal in spin space and collinear spin is assumed.[60] In Eq. (1), $\hat{T}$ is the kinetic energy, $\hat{V}^{\rm local}$ is the fully local long-ranged potential commonly set to the $l = 0$ radial component of the PP, $\hat{V}^{\rm KB}$ is the Kleinmann-Bylander (KB) operator,[57] $\hat{V}_H$ the Hartree term, and $\hat{V}_{\rm XC}$ is the exchange-correlation operator. Just two of those terms depend on the spin projections (say along the z axis) σ (=↑,↓): the KB term and the final (exchange correlation) term. In the collinear case, there is a common quantization axis for the whole system, and the charge density has two independent projections $\rho^{\uparrow}(\mathbf{r})$ and $\rho^{\downarrow}(\mathbf{r})$, parallel and antiparallel, respectively. However, in the FR-PP aproximation, off-diagonal spin terms appear in the Hamiltonian causing a mixture of spin components because the spin quantization axis varies from point to point in space, i.e., noncollinear case. Consequently, it was necessary to use the scheme developed by Kübler *et al.*[62] that will give the mixed components for XC potential (see Ref. 53 for details).

From an *ab initio* point of view, the MAE is defined as the difference in the total energy between easy and hard magnetization axes. It is common to fix the spin quantization axis as the z direction. However, when the FR-PP approximation is used and we need the total energy in several directions, it necessary to proceed in a different way, specifically to generalize the magnetization direction to an arbitrary axis $S_{\mathbf{u}}$, characterized by polar angles θ and ϕ. The procedure will give us a new set of matrix elements as a function of θ and ϕ angles for the KB term $\hat{V}^{\rm KB}_{\theta,\phi}$. For the total energy calculations required to determine the MAE, we obtain self-consistency by means of the Hamiltonian instead of using the density matrix. To this end, in each iteration the Hamiltonian is obtained after a Pulay mixing[63] of the input and output Hamiltonian $H^{\rm in}$, $H^{\rm out}$, respectively. The criterion for a self-consistent solution is the requirement that input and output values differ by less than 1 meV. For each different set of angles (θ',ϕ'), we restart the self-consistent scheme using as input Hamiltonian the one output for the previous angles (θ,ϕ):

$$H'^{,\rm in} = H^{\rm out} - V^{\rm KB}_{\theta,\phi} + V^{\rm KB}_{\theta',\phi'}, \qquad (2)$$

where the primes denote the matrices calculated for angles (θ',ϕ').

The unit cell for $L1_0$ metallic based alloys consists of two fcc cells displaced along the diagonal of the cube. The presence of two different kinds of atoms generates a vertical distortion so that its structure is defined by two quantities: the in-plane lattice parameter a and the out-of-plane constant c. Prior to relaxation, the NPs were constructed from their bulk fct phase forming a perfect $L1_0$ ordered cuboctahedron (see Fig. 1). We

have restricted our study to the so-called magic cluster sizes $N_{\text{tot}} = (10n^3 + 15n^2 + 11n + 3)/3$, where n is the number of geometrical closed shells, being the total number of atoms for each species $N_{\text{M}} = (5n^3 + 6n^2 + 4n)/3$ for magnetic (M) species Fe and Co, and $N_{\text{NM}} = (5n^3 + 9n^2 + 7n + 3)/3$ for nonmagnetic (NM) species Pt, Au, and Pd. The initial lattice parameters a, as well as the c/a ratios, were chosen as their bulk experimental values[64]: $a_{\text{FePt}} = 3.86$ Å and $(c/a)_{\text{FePt}} = 0.98$; $a_{\text{FePd}} = 3.89$ Å and $(c/a)_{\text{FePd}} = 0.938$; $a_{\text{FeAu}} = 4.08$ Å and $(c/a)_{\text{FeAu}} = 0.939$; $a_{\text{CoPt}} = 3.81$ Å and $(c/a)_{\text{CoPt}} = 0.968$.

III. RESULTS

We have carried out a systematic study of bimetallic nanoclusters, concentrating on the magnetic properties (spin and MAE). The calculations were made on fully relaxed structures produced using a conjugate gradient method. In the following sections, we present the results of the magnetic property calculations, but first we consider the structures themselves as a basis for the interpretation of the magnetic properties.

A. Conjugate gradient relaxations

To carry out relaxation of the NP structures, we have employed the conjugate gradient (CG) method, minimizing the forces between atoms until they were less than 0.03 eV/Å. The optimizations have been done at a spin-polarized SR level, and just to address the calculations of MAE, spin moments, and density of states (DOS), a FR-PP scheme was included.

In Fig. 2, we show the radial distribution function (RDF) of the evolution of the values of the lattice parameters a, c and the first-nearest-neighbor distances nn, after a CG relaxation of the (Fe,Co)Pt and Fe(Au,Pd) NPs. It is important to note that during the optimization process, no constraint was introduced on the initial positions of the NPs in order to allow all the atoms to move freely and thereby to produce a physically more realistic configuration after the relaxation. Although the NPs experience only a small reconstruction, this is enough to change the magnetic properties substantially, as we will show in Sec. III D. The dispersion in the nn values for Fe species [green thick lines in Fig. 2 (A.1–A.4)] around the bulk value is ±0.4 Å. This means that the Fe atoms have a regular distribution around nn. Additionally, this behavior is followed by the other Fe-based NPs as can be seen in Fig. 2 (C and D), especially for the bigger NPs C.3 and D.3. Regarding the nonmagnetic atoms (blue thin lines), this range is around 0.2 Å less than that of the Fe atoms and also the average displacements are smaller. As a result, the Pt, Au, and Pd atoms are concentrated closer to their bulk positions than Fe. With respect to the mean distance between planes for each species, it is interesting to note that Fe planes are closer after a reduction of the bulk value by −0.6 Å in all the Fe-based NPs. On the contrary, the distances between NM planes are larger, increasing by a mean value of 0.6 Å. In general, we can say that the magnetic species have a higher dispersion around their bulk lattice parameters than the nonmagnetic ones, except for the case of $Fe_{24}(Pt,Au,Pd)_{31}$, where Pt, Au, and Pd atoms are also significantly distributed around c and a. It can be seen that for CoPt NPs [Fig. 2 (B.1–B4)], the dispersion around a, c, and nn is less than for FePt NPs. In this case, both Co

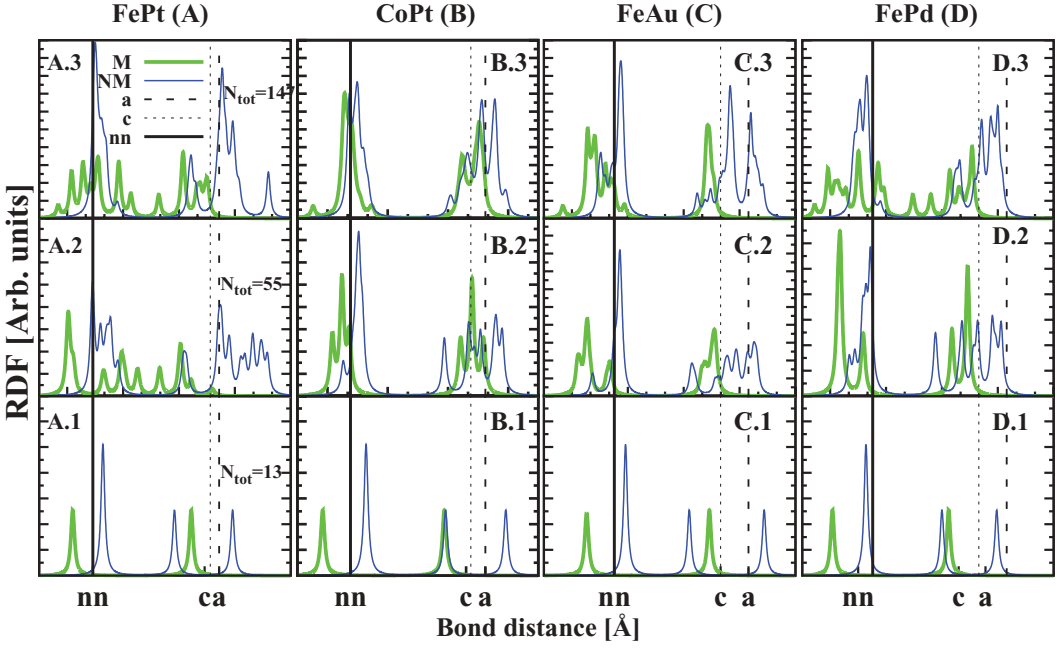

FIG. 2. (Color online) Lorentzian broadening of the bond distances between magnetic ($d_{\text{M-M}}$) and nonmagnetic ($d_{\text{NM-NM}}$) atoms, thick green (light gray) and thin blue lines (dark gray), respectively. Each one of the four columns (A,B,C,D), from bottom to top, depict the distances when the number of total atoms N_{tot} increase from 13 to 147, (A.1) to (A.3) for FePt, (B.1) to (B.3) for CoPt, (C.1) to (C.3) for FeAu, and (D.1) to (D.3) for FePd. The three vertical lines show a (black dashed), c (black dotted), and the first-nearest-neighbors nn (black solid) experimental lattice values in their bulk phases. The values are provided in the text.

and Pt atom positions deviate by ±0.15 Å from their bulk *nn* structure values. As in the FePt case, the Co atoms have reduced their mean separation values, while those of the Pt atoms have increased. The distance between planes differs by smaller amounts than for FePt, the ranges being between −0.2 and +0.3 Å for M and NM atoms. This implies that for CoPt NPs there is less distortion of the bulk structure, which is clearly shown by the opened gap between the first and the following peaks in CoPt, filled in FePt and FePd. Specifically, the Au atoms experience an increase in their *nn* distances of 0.15 Å, while the separation of Fe atoms decreases by 0.3 Å. The out of plane variations are between +0.4 Å for Au atoms and −0.3 Å for Fe atoms. It is interesting to point out that in general the distance of the surface atoms from the center of the NPs tends to be reduced in comparison with the initial bulk structures. Studying this distance for the atoms located at different types of surfaces (squares on the top and the bottom and triangles or squares in the side of the molecules) (see Fig. 1), we can say that there is not a general trend either for magnetic or nonmagnetic species.

In Fig. 3, we show the same evolution as we depicted in Fig. 2, but now in each one of the four graphs it can be seen how the bond distances between the magnetic and nonmagnetic nearest-neighbor atoms $d_{M\text{-}NM}$ have changed with respect to the bulk ones (vertical black lines) as the total number of atoms increases. It is clear that the tendency is quite similar in all of them. For instance, all the bonding values for the bigger NPs are concentrated around the bulk values, while when $N_{tot} = 13$ or 55, the peaks have displaced to shorter bonding distances, consequently decreasing the distance between M and NM planes.

As a final study, and to check the accuracy of the predicted atomic positions, we decreased the force tolerance between atoms from 30 to 8 meV/Å and additionally we reduced the self-consistency tolerance criterion to less than 10 μeV for some clusters containing either Fe or Co species. After inspecting carefully the new coordinates of each atomic species for each considered NP and analyzing the $d_{M\text{-}M}$ and $d_{M\text{-}NM}$ distribution (not shown here), we can conclude that the coordinates of the M and NM atoms have changed by less than 1 mÅ for the smaller clusters and 0.1 mÅ for the bigger ones. Consequently, we consider that the first criterion will give physically realistic metastable phases and hence it will be sufficient to carry out studies of the electronic and magnetic properties of these NPs without sacrificing accuracy.

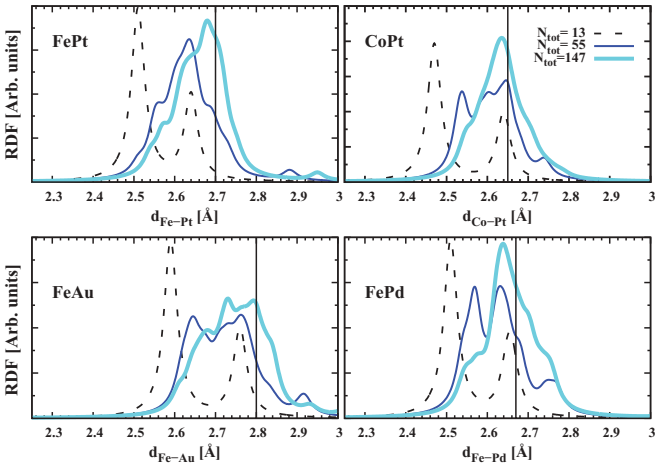

FIG. 3. (Color online) Lorentzian broadening of the nearest-neighbors bond distances between magnetic and nonmagnetic atoms ($d_{M\text{-}NM}$). In each of the four graphs, it is shown how the bonding evolves as the size of the clusters increases: $N_{tot} = 13$ (black dashed), $N_{tot} = 55$ (thin blue), and $N_{tot} = 147$ (thick turquoise).

B. Magnetic moments

As a result of a Mulliken analysis, we show in Fig. 4 the variation of the spin magnetic moment (MM) values for every atom belonging to Fe(Pt,Au,Pd) and CoPt NPs in function of its distance from the center. The MM values have been derived as the difference between the majority and minority spin charges and, although this is a qualitative study, it allows

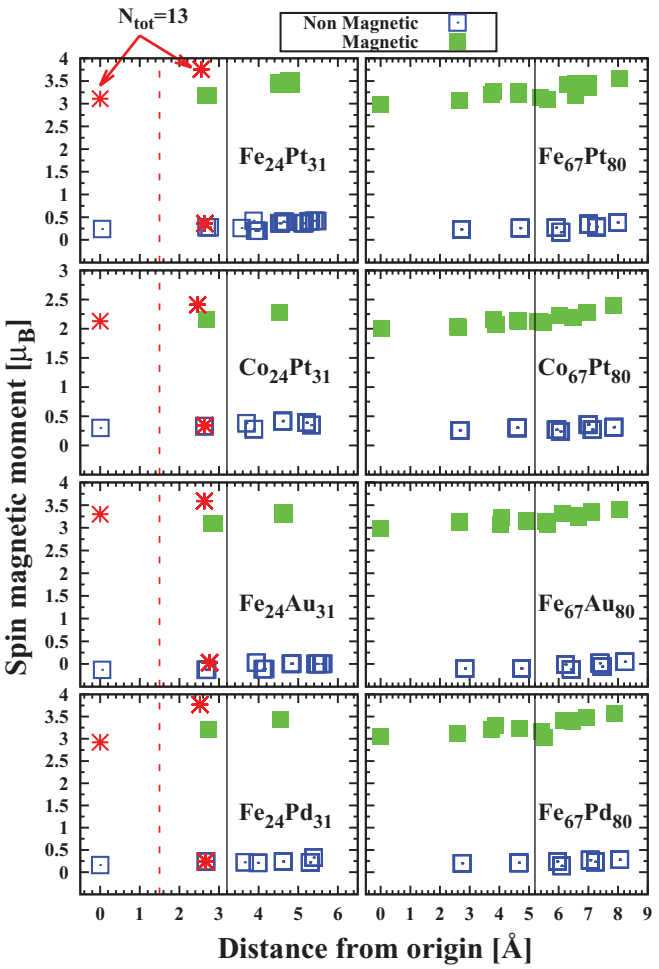

FIG. 4. (Color online) Spin magnetic moments for each kind of atom (magnetic and nonmagnetic) as a function of their distance from the center of the NP. Each row shows, from left to right, how the MM values evolve when the total number of atoms increase for a specific alloy (N_{tot} = 13, 55, 147). Fe and Co atoms are depicted by green filled squares, while Pt by empty blue ones. The red symbols show the MM values for each one of the atoms when $N_{tot} = 13$. Every graph has been divided by a solid line showing two zones that point out the core and surface regions. The added red dashed line in the first column also divides the smaller NP in the core and surface regions.

us to determine whether the NPs have more polarization in the surface or in the core.

The local MM of the Fe and Co atoms (green filled squares) are remarkably large in comparison with those of the Pt atoms (blue empty squares). This is a general trend in all the clusters and the average differences range from 1.8 to 3.3 μ_B for $Co_{67}Pt_{80}$ and $Fe_{67}Pt_{80}$, respectively. Taking into account the region where the atoms reside (core or surface), the values will be slightly different. So, we can observe that for magnetic atoms, all the NPs have their inner MM values lower than those in the surface by $\sim$0.4 μ_B. However, the Pt MM values remain around 0.25 μ_B along their radial positions, the difference being only 0.1 μ_B from inner to surface. This behavior prevails even for CoPt NPs.

It is noticeable that the Co local MM are $\sim$1.4 μ_B smaller than their magnetic counterpart in any other NP, even for Fe(Au,Pd). It is also interesting to note that the local MM at the surface in the smaller NPs (red symbols) have the largest values. The ratio of surface to volume atoms in these tiny NPs is 12/1 and 92% of the atoms are located on the surface. So, the surface effects are more pronounced at these sizes as we see in the increasing values of the MM.

In Table I, we summarize the total MM of all the NPs studied in this work. One of the main results is that for all the sizes, the FePt NPs have higher MM_{tot}/N_{tot} when compared with any other kind of NPs. The FePt values range from 1.62 μ_B/at for Fe_5Pt_8 to 1.66 μ_B/at for $Fe_{24}Pt_{31}$. Despite this small increase for MM_{tot}/N_{tot}, the different kind of NPs follow the same trend as the NP size increases. $Fe_{67}Pd_{80}$ is an exception having a value of 0.15 μ_B/at less than $Fe_{24}Pd_{31}$. On inspection of the first and the second columns of Table I, we note that the average projected MM_M/at and MM_{NM}/at values decrease as the size of the clusters increases for all NP types. This loss of MM values for the magnetic and nonmagnetic atoms as the size of the NPs increases could be due to the fact that the percentage of surface atoms decreases from 80% with increasing N_{tot}, and as we have seen in Fig. 4 the contribution of the higher spin values of the surface atoms will be diminished. It is worth noting that the magnetic atoms are not entirely responsible for the overall magnetic behavior; the contribution from the spins of nonmagnetic ones is vital to this complicated magnetic process.

C. Density of states (DOS)

To gain further insight about the electronic behavior of the NPs, we present in Fig. 5 the spin-resolved density of states (DOS) projected onto M and NM atoms for all the clusters studied in this work. The atoms have been divided into two groups as previously in this paper: surface (thick green lines and thin blue lines) and core (filled colored curves). The black lines show the total DOS.

First, we note that for all the types of NPs, as N_{tot} increases, the total DOS peaks are smeared and bands are formed implying that the electrons become delocalized. Further, the projected DOS on magnetic surface atoms, together with their core counterpart, show that they provide the largest contribution to the total MM of the NPs. The majority and minority bands of the smaller (Fe,Co)Pt and FePd type NPs (A.1, B.1, and D.1) have peaks around 0.25 eV for the first two NPs and at the Fermi level for FePd, and as the size of the NPs increases, some of these peaks move below the Fermi level. For minority states, the FePt peak moves up to -0.3 eV, and up to the Fermi level for the majority states. CoPt NPs have the same behavior only for majority states, while the minority peak remains at energies greater than E_F for larger sizes. Fe_5Pd_8 NP show this displacement until around -0.2 eV for the minority bands. These displacements imply that the d bands are filling and, as a result, there is a decrease of the total surface MM for the magnetic species of 0.4 μ_B for FePt and 0.15 μ_B for CoPt (see first row in Fig. 6) as N_{tot} increases. It is interesting to note that for the Fe(Au,Pd) smaller NPs, there is a gap that disappears as the size increases. Other features of the total majority DOS of smaller NPs are the humps at -1, -4, and at -5 eV for FePt and at -1, -3.5, and -5 eV for CoPt. The first two peaks located at higher energies persist for larger NPs, however, the last disappears when $N_{tot} > 13$. It is worth noting that the FePt NPs with $N_{tot} > 13$ have a dip in the minority DOS at the Fermi level, showing that the minority channel is dominated by Fe surface atoms. This is in good agreement with the work of Gruner *et al.* so that this feature gives a way to distinguish between different morphologies such as icosahedron or $L1_0$ cuboctahedron.[27] In general, the DOS of FePd and FeAu NPs present a slightly different shape, but nonetheless exhibit the main feature the

TABLE I. Magnetic moment (MM) values in μ_B/at of all $L1_0$ cuboctahedral based NPs as well as those obtained for the corresponding bulk alloys using the current FR-PP formalism and also the FR approximation. The first column displays the number of total atoms N_{tot} as well as the bulk. The MM values in the first and the second columns of each kind of alloyed NPs have been calculated by means of the equations MM_M/N_M and MM_{NM}/N_{NM}, respectively, whereas in the text, M refers to magnetic atoms and NM to the nonmagnetic ones. The third column shows MM_{tot}/N_{tot}.

	FePt			FePd			FeAu			CoPt		
N_{tot}	M	NM	Total	M	NM	Total	M	NM	Total	M	NM	Total
13	3.63	0.36	1.62	3.60	0.24	1.53	3.53	0.04	1.38	2.36	0.34	1.11
55	3.36	0.34	1.66	3.36	0.24	1.60	3.25	−0.03	1.40	2.24	0.36	1.18
147	3.29	0.28	1.65	3.33	0.23	1.45	3.23	−0.05	1.45	2.19	0.30	1.16
Bulk[a]	3.12	0.18	1.65	3.14	0.17	1.66	3.21	−0.17	1.52	2.00	0.29	1.15
Bulk Others[a]	2.96	0.34	1.65	3.02	0.36	1.69	3.00	0.04	1.52	1.83	0.37	1.10

[a]Reference 53.

[a]Reference 64.

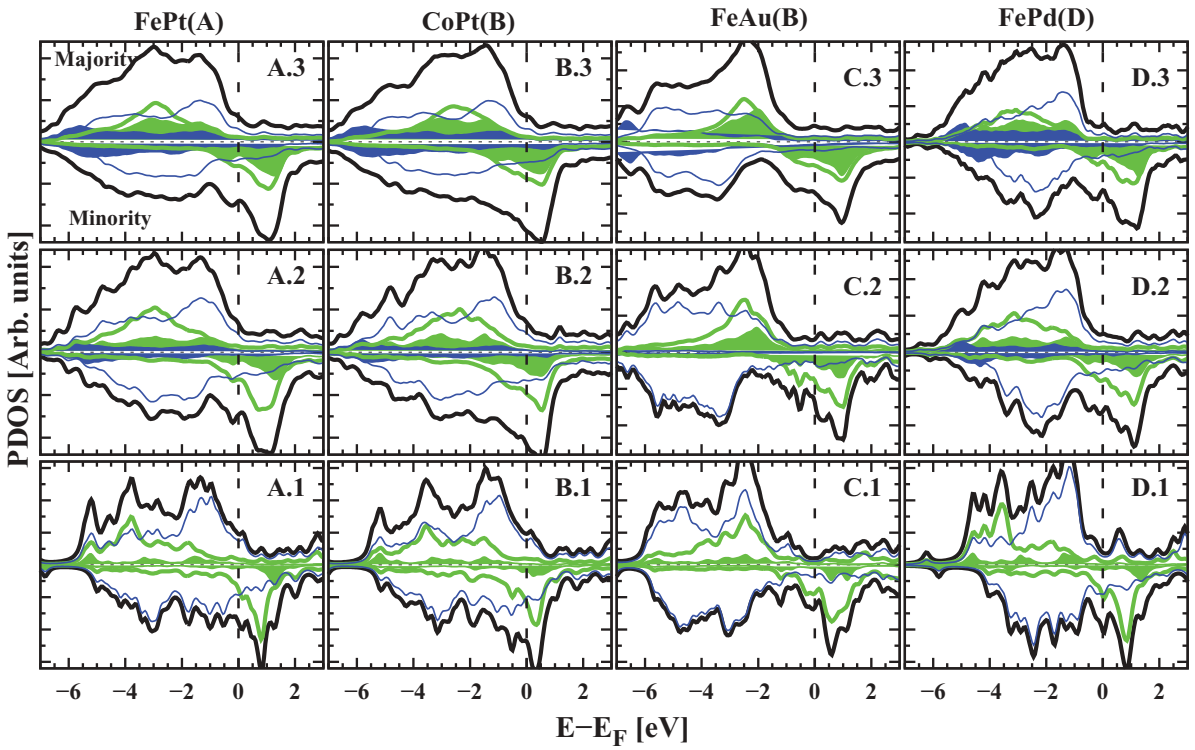

FIG. 5. (Color online) Spin-resolved density of states (DOS) of FePt (A.1-3), CoPt (B.1-3), FeAu (C.1-3), and FePd (D.1-3) alloyed NPs. Full black lines show the total up and down DOS when the total number of atoms N_{tot} varies from 13 to 147 from bottom to top. The projected DOS of the surface atoms are represented by thick solid green lines for Fe and Co atoms and thin solid blue lines for the Pt, Au, and Pd atoms. The filled curves show the projected DOS for the core M and NM atoms, green and blue, respectively.

primary responsibility of the M atoms for the polarization in these NPs as well.

D. Magnetic anisotropy

We finally present the calculations of the magnetic anisotropy (MAE). In order to get a better knowledge of the magnetic behavior of the NPs, we also show in Fig. 6, together with the MAE, the MM for Fe, Co, Pt, Pd, and Au atoms in the first and second rows. It is easy to distinguish between the MM of the surface and core atoms, whether or not they are magnetic, since as we have seen in Sec. III B that the local surface MM values are higher than those of the core.

Although there are some common tendencies in the behavior, there is no overall trend, presumably because of the complexity of the atomic rearrangements and charge transfer. Consider first the behavior of the MM values of the magnetic atoms in FePt, CoPt, FePd, and FeAu. The common factor in the behavior of all systems is an increase of the MM in the surface over that of the core atoms. In addition, FePt, CoPt, and FePd exhibit large differences (as large as $\Delta\mu = 0.7\ \mu_B$/at for FePt), which decreases with increasing N_{tot}. The similarity presumably reflects the chemical similarity of Pd and Pt. Although its surface atoms have a larger MM than the core atoms, FeAu breaks the trend in that $\Delta\mu$ remains reasonably constant, presumably reflecting the different atomic rearrangements and charge transfer. Turning to the MM values of the nonmagnetic species, the tendency of the MM is to be almost constant within both the core and surface regions. Again, we note that the nonmagnetic atoms of FeAu NPs exhibit a different trend, and that further their MM values for $N_{\text{tot}} = 55, 147$ are negative.

The calculated values of the MAE are shown in Fig. 6 (A.1, B.1). The alloys from which our NPs have been constructed have in their bulk $L1_0$ phases a MAE of order of a few meV (Ref. 64) with the easy magnetization axis perpendicular to the atomic planes (see Fig. 1). We will see that most of all the studied NPs have the same easy axis orientation as their bulk alloys. Also, the values of the total MAE obtained in this work are of order of tens of meV following the same trend shown by other groups for small NPs.[30,31] In the graphs, the MAE is expressed in meV per atom by dividing by the total number of atoms (magnetic plus nonmagnetic) of each NP, and using straight colored lines we show the MAE values for each $L1_0$ alloy.

Consider first the case of FePt and CoPt shown in Fig. 6 (A.1). Although we do not have site-resolved MAE values, we can interpret the data in relation to previous calculations of bulk properties of FePt.[70,71] These suggest that the primary contribution to the MAE in FePt is a two-ion anisotropy of the Fe sites mediated by the Pt sites. This suggests that the presence of surfaces and the consequent loss of coordination might be expected to lower the overall MAE, which is certainly the case for the two larger NP sizes considered here. However, it is interesting to note that the smallest NP size exhibits an increased MAE. Although we can not here obtain site-resolved information for the MAE, it seems reasonable to suggest that this arises from the modified electronic properties within the

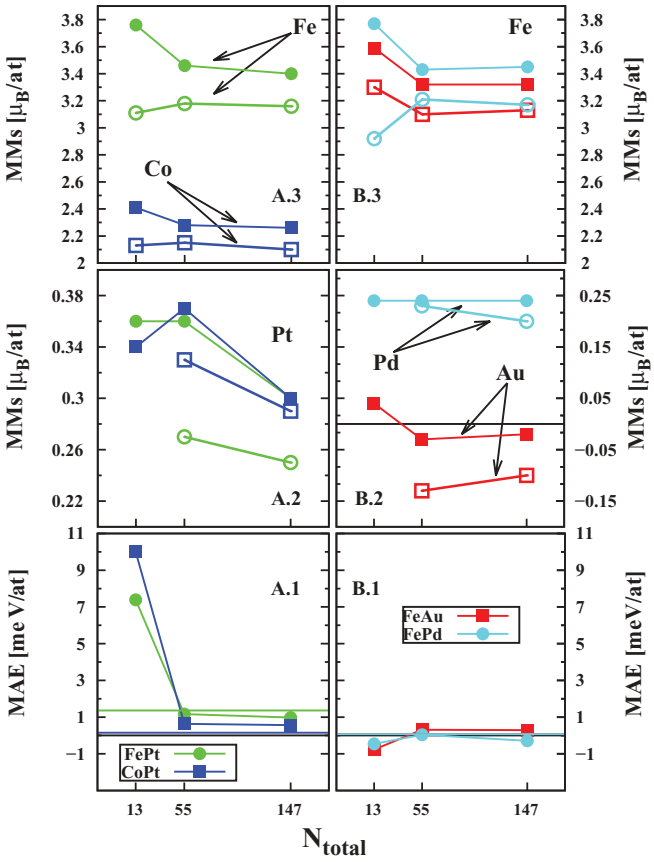

FIG. 6. (Color online) Magnetic anisotropy (MAE) values per atom and mean surface and core magnetic moments (MM) values per atom for Fe, Co, Au, Pd, and Pt of FePt (green), CoPt (blue), FeAu (red), and FePd (turquoise) NPs as a function of their total number of atoms. The unfilled symbols represent the core MM values, while the filled ones correspond to the surface MM.

smallest NPs. This is worth further consideration, with site-resolved calculations, since this enhanced MAE may be useful for applications.

It is also interesting to compare the values obtained in this work with those obtained previously for the bulk $L1_0$ alloys with the same code[53] as well as those with other implementations and also experimental values. To this end, we provide in Table II a comparison of the MAE values when different implementations have been used (for a deeper comparison of the explicit XC functionals and kind of approximations, see Ref. 53 and references therein).

Regarding the orientation of the easy axis, most of the NPs studied present easy axis along the Z axis. However, we note that for Fe_5Pd_8, Fe_5Au_8, and $Fe_{67}Pd_{80}$ the MAE has a negative value which means that the easy axis lies in the XY plane. Further evidence of contributions to the MAE beyond the simple uniaxial case is shown in Fig. 7. Here, we show the variation of the total energy of the $Fe_{24}Pt_{31}$ (upper row) and $Co_{24}Pt_{31}$ (lower row) NPs with the θ (left) and ϕ (right) angles. In both types of NPs, the easy magnetization axis lies along the (001) direction, having the minimum value of the energy ($\theta = 0^\circ, \phi = 0^\circ$). Fixing ϕ to 0° (empty blue squares) and 45° (full green dots) and varying θ from zero to 180°, we obtained different maxima for $Co_{24}Pt_{31}$ while the $Fe_{24}Pt_{31}$ NPs exhibit

TABLE II. MAE for the $L1_0$ alloyed (Fe,Co)Pt and Fe(Au,Pd) NPs as well the calculated former values for the bulk phases using the current approximation. Other bulk MAE values given by other groups and also the experimental ones have been shown in the last two rows. All the values are in meV/at.

	MAE			
N_{tot}	FePt	FePd	FeAu	CoPt
13	7.4	−0.5	0.8	10
55	1.2	0.04	0.3	0.6
147	1.0	0.3	0.3	0.6
Bulk[a]	1.4	0.05	0.1	0.2
Bulk Others	2.0[b],1.8[c]	−0.5[b],0.15[d]	0.6[b]	0.9[b],1.0[c]
Experimental	1.2[e]	0.4[f]		1.0[g]

[a]Reference 53.
[b]Reference 64.
[c]Reference 65.
[d]Reference 66.
[e]Reference 67.
[f]Reference 68.
[g]Reference 69.

purely uniaxial behavior, with no dependence of ϕ. The graphs on the right side sweep the energy from $\phi = 0^\circ$ to 180° keeping θ constant. It can be seen that the in-plane magnetization for CoPt has two minima exactly at 45° and at 135° (see Fig. 1). In the case of FePt NPs, no in-plane anisotropy is observed.

IV. CONCLUSIONS

In conclusion, we have carried out fully relativistic calculations, within the GGA approximation, of the magnetic moments, density of states, and MAE of $L1_0$ cuboctahedral FePt-, CoPt-, FeAu-, and FePd-based NPs. We have restricted the total number of atoms to the magic numbers: 13, 55, and 147, giving diameters of the NPs from 0.6 nm for $N_{tot} = 13$ up to 1.6 nm for $N_{tot} = 147$.

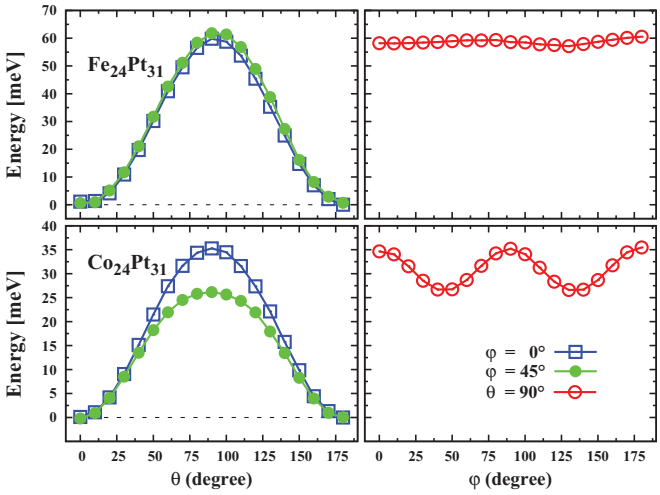

FIG. 7. (Color online) Energy variation as a function of the θ (left) and ϕ (right) angles for $Fe_{24}Pt_{31}$ and $Co_{24}Pt_{31}$ NPs in the upper and lower rows, respectively. The zero of energy is set to the minimum value of E and all the points have been joined with lines in order to guide the eye.

Although the original stacking is retained after CG relaxation, the atoms exhibit small displacements from their original bulk positions. The bond distances between magnetic species have higher dispersion around the characteristic bulk values than exhibited by nonmagnetic atoms, the nonmagnetic species being almost at the same position. Although this trend is followed by most of the NPs, there is an exception for CoPt NPs that shows much less dispersion for both magnetic and nonmagnetic species.

Regarding the magnetic structure, we have shown that the outermost local magnetic moments of all the NPs studied in this work are larger than in the core, in good agreement with previous investigations. This magnetic behavior is correlated with the PDOS analysis that shows the importance of the magnetic ordering of the surface magnetic species polarization. Also, we showed that the MAE is size and stacking dependent and that the value increases for the smallest NPs with respect to the bulk values. This indicates enhanced thermal stability of the smallest NPs. However, the larger FePt and CoPt NPs showed a reduction of the MAE consistent with the loss of coordination at the surface and a consequent reduction of the (dominant) two-ion anisotropy. This is an interesting observation which shows a dramatic change in the magnetic behavior in the smallest NPs, which is worth investigating using site-resolved MAE calculations.

The easy magnetization axis generally lies along the (001) direction, although in some FeAu and FePd NPs the anisotropy lies in plane. As an example of an in-plane magnetic anisotropy, we obtained θ and ϕ energy dependence for $(Fe,Co)_{24}Pt_{31}$ NPs in Fig. 7 showing that the surface shape is important to study the entire energy surface to investigate the overall form of the MAE, which, certainly for the case of $Co_{24}Pt_{31}$, has a significant contribution from a cubic anisotropy term in addition to the main uniaxial term.

ACKNOWLEDGMENTS

The authors would like to acknowledge helpful discussions with T. J. Klemmer. The financial support of Seagate Technology and the EU FP7 programme [Grants No. NMP3-SL-2008-214469 (UltraMagnetron) and No. 214810 (FANTOMAS)] is also gratefully acknowledged.

[1] Q. A. Pankhurst, J. Connolly, S. K. Jones, and J. Dobson, J. Phys. D: Appl. Phys. **36**, R167 (2003).
[2] O. Salata, J. Nanobiotechnology **2**, 3 (2004).
[3] C. C. Berry and S. G. Curtis, J. Phys. D.: Appl. Phys. **36**, R198 (2003).
[4] S. Zyade, F. Garin, and G. Maire, New J. Chem. **11**, 429 (1987).
[5] N. Jones, Nature (London) **472**, 22 (2011).
[6] O. Gutfleisch, L. Lyubina, K. H. Muller, and L. Schultz, Adv. Eng. Mater. **7**, 208 (2005).
[7] B. D. Terris and T. Thomson, J. Phys. D: Appl. Phys. **38**, R199 (2005).
[8] C. A. Ross, Annu. Rev. Mater. Sci. **31**, 203 (2001).
[9] Y. F. Xu, M. L. Yan, and D. J. Sellmyer, J. Nanosci. Nanotechnol. **7**, 206 (2007).
[10] D. Weller and A. Moser, IEEE Trans. Magn. **35**, 4423 (1999).
[11] H. Zeng, J. Li, P. Liu, Z. L Wang, and S. Sun, Nature (London) **420**, 395 (2002).
[12] A. Y. Dobin and H. J. Richter, Appl. Phys. Lett. **89**, 062512 (2006).
[13] S. Greaves, Y. Kanai, and H. Murakoa, IEEE Trans. Magn. **43**, 2118 (2007).
[14] R. E. Rottmayer, S. Batra, D. Buechel, W. A. Challener, J. Hohlfeld, Y. Kubota, Lei Li, Bin Lu, C. Mihalcea, K. Mountfield, K. Pelhos, Chubing Peng, T. Rausch, M. A. Seigler, D. Weller, and XiaoMin Yang, IEEE Trans. Magn. **42**, 2417 (2006).
[15] C. Verdes, R. W. Chantrell, A. Satoh, J. W. Harrell, and D. Nikles, J. Magn. Magn. Mater. **304**, 27 (2006).
[16] J. Kohlhepp and U. Gradmann, J. Magn. Magn. Mater. **139**, 347 (1995).
[17] B. Revaz, M. C. Cyrille, B. Zink, I. K. Schuller, and F. Hellman, Phys. Rev. B **65**, 094417 (2002).
[18] J. Lindner, C. Rüdt, E. Kosubek, P. Poulopoulos, K. Baberschke, P. Blomquist, R. Wäppling, and D. L. Mills, Phys. Rev. Lett. **88**, 167206 (2002).
[19] Roman V. Chepulskii and W. H. Butler, Appl. Phys. Lett. **100**, 142405 (2012).
[20] P. Gambardella, S. Rusponi, M. Veronese, S. S. Dhesi, C. Grazioli, A. Dallmeyer, I. Cabria, R. Zeller, P. H. Dededrich, K. Kern, C. Carbone, and H. Brune, Science **300**, 1130 (2003).
[21] Ji-Zhou Kong, You-Pin Gong, Xue-Fei Li, Ai-Dong Li, Jun-Long Zhang, Qing-Yu Yan, and Di Wu, J. Mater. Chem. **21**, 5046 (2011).
[22] Q. Yan, A. Purkayastha, A. P. Singh, H. Li, A. Li, R. V. Ramanujan, and G. Ramanath, Nanotechnology **20**, 025609 (2009).
[23] G. M. Pastor, J. Dorantes-Dávila, S. Pick, and H. Dreysse, Phys. Rev. Lett. **75**, 326 (1995).
[24] Y. Tamada, S. Yamamoto, S. Nasu, and T. Ono, J. Phys.: Conf. Ser. **200**, 072098 (2010).
[25] T. Thomson, M. F. Toney, S. Raoux, S. L. Lee, S. Sun, C. B. Murray, and B. D. Terris, J. Appl. Phys. **96**, 1197 (2004).
[26] Sebastian Loth, Susanne Baumann, Christopher P. Lutz, D. M. Eigler, and Andreas J. Heinrich, Science **335**, 196 (2012).
[27] Georg Rollmann, Markus E. Gruner, Alfred Hucht, Ralf Meyer, Peter Entel, Murilo L. Tiago, and James R. Chelikowsky, Phys. Rev. Lett. **99**, 083402 (2007).
[28] Markus E. Gruner, Georg Rollmann, Peter Entel, and Michael Farle, Phys. Rev. Lett. **100**, 087203 (2008).
[29] Ranber Singh and Peter Kroll, Phys. Rev. B **78**, 245404 (2008).
[30] Lucas Fernández–Seivane and Jaime Ferrer, Phys. Rev. Lett. **99**, 183401 (2007).
[31] S. Sahoo, A. Hucht, M. E. Gruner, G. Rollmann, P. Entel, A. Postnikov, J. Ferrer, L. Fernández–Seivane, M. Richter, D. Fritsch, and S. Sil, Phys. Rev. B **82**, 054418 (2010).
[32] O. A. Ivanov, L. V. Solina, V. A. Demshina, and L. M Magat, Fiz. Met. Metalloyed **35**, 92 (1973).
[33] C. Antoniak, J. Lindner, M. Spasova, D. Sudfeld, M. Acet, M. Farle, K. Fauth, U. Wiedwald, H.-G. Boyen, P. Ziemann, F. Wilhelm, A. Rogalev, and S. Sun, Phys. Rev. Lett. **97**, 117201 (2006).
[34] R. Wang, O. Dmitrieva, M. Farle, G. Dumpich, H. Q. Ye, H. Poppa, R. Kilaas, and C. Kisielowski, Phys. Rev. Lett. **100**, 017205 (2008).
[35] L. Néel, J. Phys. Radium **15**, 376 (1954).

[36]J. Stöhr and H. C. Siegmann, *Magnetism* (Springer, Berlin, 2006).
[37]Y. Wang, B. Ding, H. Li, X. Zhang, B. Cai, and Y. Zhang, J. Magn. Magn. Mater. **308**, 108 (2007).
[38]S. Kang, Z. Jia, I. Zoto, D. Reed, D. E. Nikles, J. W. Harrell, G. Thompson, and G. Mankey, J. Appl. Phys. **99**, 08N704 (2006).
[39]S. Hong and M. H. Yoo, J. Appl. Phys. **97**, 084315 (2005).
[40]C. Zhou, T. C. Schulthess, and O. Mryasov, IEEE Trans. Magn. **43**, 2950 (2007).
[41]Markus E. Gruner, J. Phys. D: Appl. Phys. **41**, 134015 (2008).
[42]P. Entel and M. E. Gruner, J. Phys.: Condens. Matter **21**, 064228 (2009).
[43]Carolin Antoniak, Markus E. Gruner, Marina Spasova, Anastasia V. Trunova, Florian Römer, Anne Warland, Bernhard Krumme, Kai Fauth, Shoheng Sun, Peter Entel, Michael Farle, and Heiko Wende, Nat. Commun. **2**, 528 (2011).
[44]M. E. Gruner, J. Phys. D: Appl. Phys. **43**, 474008 (2010).
[45]L. Kleinman, Phys. Rev. B **21**, 2630 (1980).
[46]D. R. Hamann, M. Schlüter, and C. Chiang, Phys. Rev. Lett. **43**, 1494 (1979).
[47]M. S. Hybertsen and S. G. Louie, Phys. Rev. B **34**, 2920 (1986).
[48]K. M. Rabe and J. D. Joannopoulos, Phys. Rev. B **32**, 2302 (1985).
[49]A. Dal Corso and A. Mosca Conte, Phys. Rev. B **71**, 115106 (2005).
[50]L. A. Hemstreet, C. Y. Fong, and J. S. Nelson, Phys. Rev. B **47**, 4238 (1993).
[51]D. Naveh, L. Kronik, M. L. Tiago, and J. R. Chelikowsky, Phys. Rev. B **76**, 153407 (2007).
[52]L. Fernández-Seivane, M. A. Oliveira, S. Sanvito, and J. Ferrer, J. Phys.: Condens. Matter **18**, 7999 (2006).
[53]R. Cuadrado and J. I. Cerdá, J. Phys.: Condens. Matter **24**, 086005 (2012).
[54]J. M. Soler, E. Artacho, J. D. Gale, A. García, J. Junquera, P. Ordejón, and D. Sánchez-Portal, J. Phys.: Condens. Matter **14**, 2745 (2002).
[55]J. I. Cerdá, M. A. Van Hove, P. Sautet, and M. Salmerón, Phys. Rev. B **56**, 15885 (1997).
[56]J. I. Cerdá, http://www.icmm.csic.es/jcerda/
[57]L. Kleinman and D. M. Bylander, Phys. Rev. Lett. **48**, 1425 (1982).
[58]N. Troullier and J. L. Martins, Phys. Rev. B **43**, 1993 (1991).
[59]J. P. Perdew, K. Burke, and M. Ernzerhof, Phys. Rev. Lett. **77**, 3865 (1996).
[60]U. von Barth and L. Hedin, J. Phys. C: Solid State Phys. **5**, 1629 (1972).
[61]S. G. Louie, S. Froyen, and M. L. Cohen, Phys. Rev. B **26**, 1738 (1982).
[62]J. Kübler, K.-H. Höck, J. Sticht, and A. R. Williams, J. Phys. F: Met. Phys. **18**, 469 (1988).
[63]P. Pulay, Chem. Phys. Lett. **73**, 393 (1980).
[64]I. Galanakis, M. Alouani, and H. Dreysse, Phys. Rev. B **62**, 6475 (2000).
[65]G. H. O. Daalderop, P. J. Kelly, and M. F. H. Schuurmans, Phys. Rev. B **44**, 12054 (1991).
[66]P. Ravindran, A. Kjekshus, H. Fjellvaag, P. James, L. Nordström, B. Johansson, and O. Eriksson, Phys. Rev. B **63**, 144409 (2001).
[67]J.-U. Thiele, L. Folks, M. L. Toney, and D. K. Weller, J. Appl. Phys. **84**, 5686 (1998).
[68]P. Kamp, A. Marty, B. Gilles, R. Hoffmann, S. Marchesini, M. Belakhovsky, C. Boeglin, H. A. Dürr, S. S. Dhesi, G. van der Laan, and A. Rogalev, Phys. Rev. B **59**, 1105 (1999).
[69]W. Grange, I. Galanakis, M. Alouani, M. Maret, J.-P. Kappler, and A. Rogalev, Phys. Rev. B **62**, 1157 (2000).
[70]J. B. Staunton, S. Ostanin, S. S. A. Razee, B. L. Gyorffy, L. Szunyogh, B. Ginatempo, and E. Bruno, Phys. Rev. Lett. **93**, 257204 (2004).
[71]O. N. Mryasov, U. Nowak, K. Y. Guslienko, and R. W. Chantrell, Europhys. Lett. **69**, 805 (2005).